Supporting information

Sequential CD34 cell fractionation by magnetophoresis in a magnetic dipole flow sorter

Thomas Schneider, Stephan Karl, Lee Robert Moore, Jeffrey John Chalmers[#]*, Philip Stephen Williams, Maciej Zborowski*[*]

Department of Biomedical Engineering, Lerner Research Institute, Cleveland Clinic, 9500 Euclid Avenue, Cleveland, Ohio 44195, USA.

[#] Department of Chemical and Biomolecular Engineering, The Ohio State University, Columbus Ohio, USA

*email: zborowm@ccf.org, tel: (216) 445-9330, fax: (216) 444-9198

CTV principle details

The CTV system used in the present study was a similar but updated version to those reported earlier. The CTV system consisted of a borosilicate glass channel (depth × height × length: 0.7 mm × 1.7 mm × 100 mm, wall thickness 0.4 mm; VitroCom) which was placed in the interpolar gap of a dipole magnet and supported by aluminium plates. A horizontally-mounted microscope (model BXFM-F; Olympus Corporation, Tokyo, Japan) contained a C-mount adaptor for video camera attachment. A 5× microscope objective was oriented so that its focal plane is approximately centered in a depth of 0.7 mm with respect to the outer channel wall. A precision lab jack and two stacked horizontal translation stages (each with vernier micrometers having 1 micrometer resolution; SM-25) were used for the 3-D positioning of the channel and magnet with respect to the microscope. A high-sensitivity, monochrome CCD camera (Retiga Exi; 2/3" optical format, 1392 × 1040 pixel resolution; QImaging Corporation, Surrey, BC, Canada) was used to capture cell motion within the magnetic field. The digital images were streamed directly to RAM via IEEE 1394 interface (firewire; at up to 20 frames/sec) and stored by a real-time disk recording software. The channel was flushed prior sample injection and measurement with 60 ml labeling buffer or 1 × PBS at high flow rate to ensure removal of contamitanting magnetic cell populations of previous measurements. The flush fluid was completely removed and the cell sample was injected in a concentration of 1×10^5 cells / ml. Up to 30 sets of measurements were performed for each sample comprising up to 40 images taken with frame delays of 100 to 1000 ms. This allowed the acquisition of at least 200 and up to 1000 tracked cells per sample. Subsequent data analysis was performed by proprietary software, internally referred to as "Imageview", that processed the images stored on the computer hard drive to yield velocity data

for each tracked cell. EXCEL macros (Microsoft Corp., Redmond, WA, USA) were used to convert the raw velocity data to histograms and to calculate statistics.

Predicting recoveries and outlet compositions from the equations of motion

The magnetic force on a labeled cell or particle, $\mathbf{F}_m$, can be approximated from that of an induced dipole. The widely reported equation is:

$$\mathbf{F}_m = V\left(M_p - \chi_f \frac{B}{\mu_0}\right)\nabla B \qquad \text{(S1)}$$

where V is the particle volume, M_p is the particle magnetization, χ_f is the susceptibility of the solution, B and ∇B is the magnetic field and its gradient, μ_0 is the permeability of free space, and vector quantities are indicated by bold typeface. For small particles with radius r in a viscous media of viscosity η, the inertial term in Newton's second law becomes approximately zero. Inside the dipole magnetic flow fractionator (DMF) the only significant components of the magnetic field gradient are along the x and y axes, and therefore $\nabla B = \frac{\partial B}{\partial x}\mathbf{e}_x + \frac{\partial B}{\partial y}\mathbf{e}_y$, where $\mathbf{e}_x$ and $\mathbf{e}_y$ are the unit vectors along the x and y axes, respectively (see Figure S2 bottom). Hence, the magnetic force essentially balances Stokes drag leading to the magnetically induced velocity:

$$\mathbf{u}_m = \frac{V\left(M_p - \chi_f \frac{B}{\mu_0}\right)}{6\pi\eta r}\nabla B \qquad \text{(S2)}$$

Here, the denominator constitutes the drag coefficient. The ratio of magnetic velocities in the DMF, u_m, to that in some other device, in particular the cell tracking Velocimeter (CTV) used to measure the magnetic cell velocity in suspension, $u_m(CTV)$, becomes

$$u_m = \frac{\eta(CTV)}{\eta}\frac{|\nabla B|}{|\nabla B(CTV)|}\frac{\left(M_p - \chi_f \frac{B}{\mu_0}\right)}{\left(M_p(CTV) - \chi_f(CTV)\frac{B(CTV)}{\mu_0}\right)}u_m(CTV) \qquad \text{(S3)}$$

where $|\nabla B| = \sqrt{\left(\frac{\partial B}{\partial x}\right)^2 + \left(\frac{\partial B}{\partial y}\right)^2}$ is the magnitude of the gradient B and $|\nabla B(CTV)|$ is that inside the region of interest of the CTV apparatus. Similarly, other references to CTV in the above formula relate to quantities measured inside the CTV apparatus. The viscosity term will cancel since the magnetically labelled cells are fractionated and analyzed in the same media in both DMF and CTV. Furthermore, we will assume that the term comprising suspending medium magnetization will be relatively small and can be neglected. The colloid used to label the cells is typically composed of magnetite, which saturates at flux densities much lower than those obtained in CTV and DMF (i.e., >1 T). Thus, M_p can be replaced with a saturation magnetization variable, which cancels from the equation. Equation S3 simplfies to

$$u_m = u_m(CTV)\frac{|\nabla B|}{|\nabla B(CTV)|} \tag{S4}$$

The gradient $|\nabla B(CTV)|$ in the CTV system refers to an average value and the normalized velocity reported from the CTV measurement is converted to mobility according to

$$u_m = m\, S_m \tag{S5}$$

where m is the magnetophoretic mobility and S_m is the force field strength, defined as $\frac{1}{2\mu_0}|\nabla B^2|$.

Note that S_m is nearly constant in the CTV apparatus, and a single value is used in the calculations. We may then write the magnet velocity components of a labelled cell in the DMF as:

$$\frac{dx}{dt} = \frac{m\, S_m}{|\nabla B(CTV)|}\frac{\partial B}{\partial x} \tag{S6}$$

$$\frac{dy}{dt} = \frac{m\, S_m}{|\nabla B(CTV)|}\frac{\partial B}{\partial y} \tag{S7}$$

Assuming no magnetic gradient for the vertical component of the velocity in the interval $z = 0$ .. L, the velocity in z direction is the superposition of particle sedimentation and convective flow:

$$\frac{dz}{dt} = w(x,y) + w_{sed} \tag{S8}$$

The velocity profile *w(x,y)* is found from

$$w(x,y) = w_{\max}\left(1 - X^2\right)\left(1 - \frac{\cosh\left(\sqrt{3}(b/w)Y\right) - 1}{\cosh\left(\sqrt{3}(b/w)\right) - 1}\right) \tag{S9}$$

where w_{max} is the maximum velocity at the center of the channel, and b/w is the aspect ratio of the channel. With the origin at the center of the channel, X is the reduced distance from the channel center along the x-axis ($X = 2x/w$, so that X ranges from -1 to +1 across the channel thickness), Y is the reduced distance from the channel center along the y-axis ($Y = 2y/b$, and Y ranges from -1 to +1 across the channel breadth).

The three parametric equations of S6-S8 can be reduced to two trajectory equations, by eliminating dt:

$$\frac{dx}{dz} = \frac{m\,S_m}{w(x,y) + w_{sed}} \frac{1}{\left|\nabla B(CTV)\right|} \frac{\partial B}{\partial x} \tag{S10}$$

$$\frac{dy}{dz} = \frac{m\,S_m}{w(x,y) + w_{sed}} \frac{1}{\left|\nabla B(CTV)\right|} \frac{\partial B}{\partial y} \tag{S11}$$

The flux density derivatives in equations S10 and S11 require maps of B in the space inside the channel and which were obtained from a 2D model of the DMF magnet assembly using MAGNETO (Integrated Engineering Software, Winnipeg, Manitoba, Canada). The 2D approximation was deemed suitable, since the magnet dimensions in the interpolar gap are small compared to the length (2.63 mm versus 76.2 mm). The MAGNETO output was calibrated

against measurements of the physical magnet with a Gauss meter and Hall probe along the midplane of the magnet gap at $x = 0$ (see methods part of the main text). The MAGNETO software was then used to predict B in a matrix of closely spaced intervals in a 2D area slightly larger than the channel ($x - y$ plane). The derivatives of dB/dx and dB/dy were found by fitting 5^{th} order Lagrange interpolating formulas and the results were stored in additional matrices in Maple.

For the trajectory modelling we assumed that the 2D magnetic field was independent of z, when z is between 0 and the length, L, of the magnet, and 0 when $z < 0$ and $z > L$. To account for the profile of the injected sample, the Maple code reads in an external file that was the output of a CFX 10 fluid flow model. This file contained a collection of points demarcating the boundary between the feed and the carrier on the x - y plane at $z = 0$.

The trajectory modeling subroutine comprised 4 loops. In the first loop, the program read in mobility-frequency pairs from the CTV analysis of the cell sample. In the second and third loops, the trajectories were seeded on a rectangular grid on the x - y plane at $z = 0$. The seed rectangle was made deliberately larger than the feed section, so a subroutine decides if a particular seeded location lies within the boundary between the feed and carrier. If so, the trajectory analysis proceeded; otherwise a new seed position was processed.

The fourth loop was the trajectory solver. The cell trajectory differential equations were solved numerically with Maple V using a Runge-Kutta method. The solution gave the x and y position for independent variables of z. A z value was substituted into the internal numeric solution if the value was too large; thus, in the loop, z is gradually increased and the returned x and y positions were compared with those of the channel's physical boundaries: the channel wall (x = half-width) and the end of the magnet ($z = L$). An external subroutine to the solver estimated the subsequent

step sizes to find the minimum z-step that will result in the particle reaching either the side wall or back wall from its last position. The algorithm used a simplified form of equations S10 and S11, where the maximum flux density derivatives were always used, and one of the variables in the velocity profile equation was held constant. Of the two *z*-steps predicted by the subroutine, the smaller was retained, which was then added to the preceding *z* estimate and the new *z* estimate was processed by the Runge-Kutta internal solution. The solver loop proceeded until either a wall boundary was substantially reached or the trial *z* exceeded *L*. If the cell reached a wall it was regarded as lost; otherwise, the *x* - *y* position at $z = L$ was evaluated and compared to the splitting planes bounding the outlet flows (eq. 3 of the main text) to determine which outlet recovers the cell.

Each trajectory terminus was weighted by the product of the frequency of the mobility increment and normalized fluid velocity at the trajectory origin at $z = 0$. The normalized velocity is defined as the local velocity (eq. 3) divided by the mean velocity. The sum of the weighing factors accrued to each outlet divided by the sum of the sample feed weighting factors subsequently gave then the individual outlet recoveries.

The same trajectory subroutine created a 2D array indexed by the number of mobility divisions and the number of outlets, plus the wall. As each mobility-frequency pair was processed by the solver, the array contents were assigned by weights of the product of composition frequency and initial velocity. In this manner, the mobility composition in each outlet – plus the wall – was predicted. The sum of the frequencies distributed across all outlets was unity, as it was the feed. With outlet compositions known, it was straightforward to calculate the mean and standard deviation in mobility in each outlet. From this followed the calculation of resolutions between adjacent outlets, and the mobility-based fractionating power in the feed, the outlets and the wall.

A detailed schematic and flowchart of the DMF setup is given in Figures S1 and S2, while a photograph of the setup is shown in Figure S3. A flowchart of data acquisition used in comparsion to the model is presented in Figure S4.

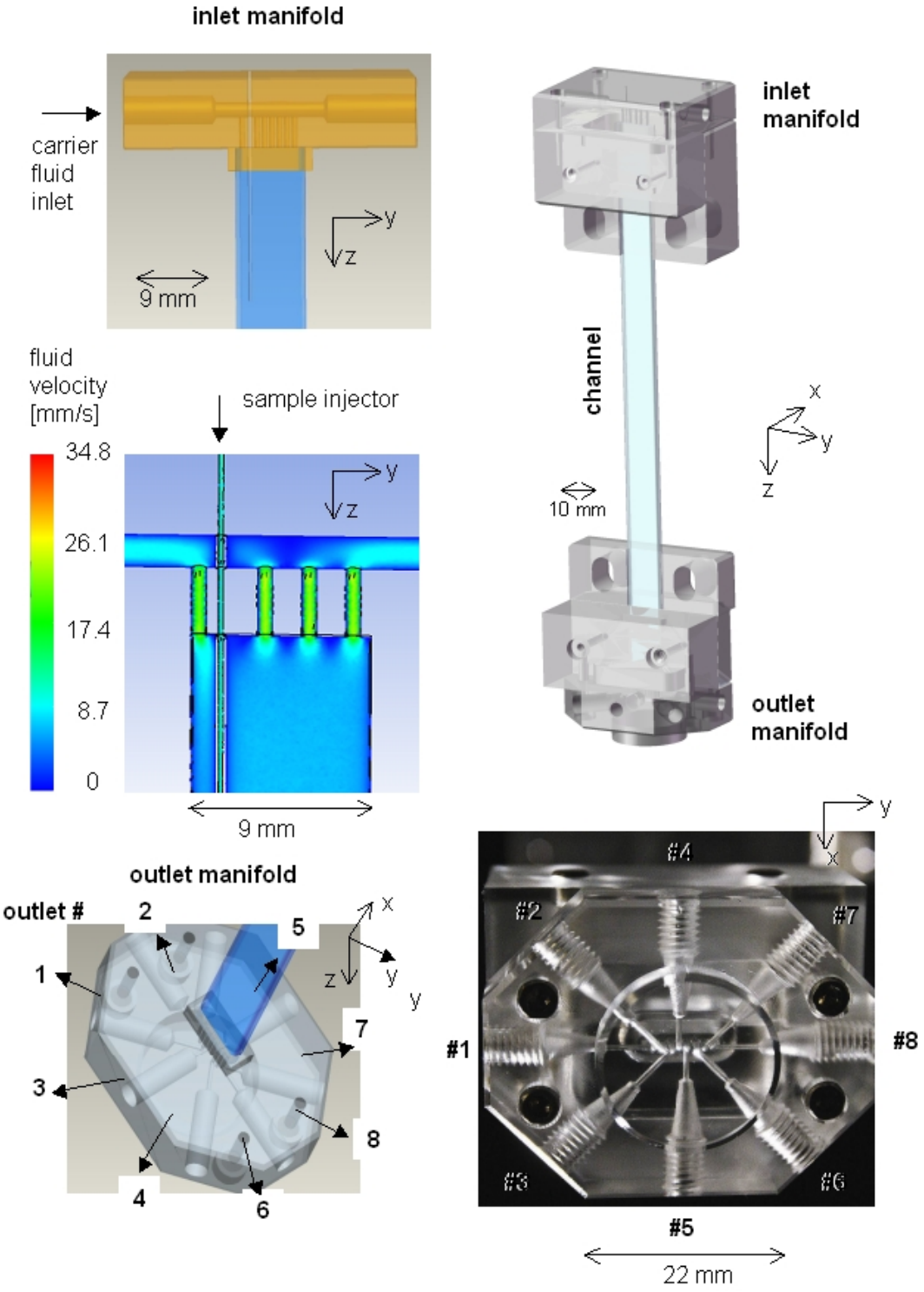

Figure S1. Counterclockwise from top right: the perspective rendering of the flow channel showing inlet and outlet manifolds with their fixtures; the detail of the inlet manifold; fluid velocity distribution in the inlet manifold showing uniform flow in the channel at the sample injector tip; perspective rendering of the outlet manifold; and the photograph of the outlet manifold from below showing details of the chromatography-type fluidic contact between the eight channel outlets with the connecting tubing.

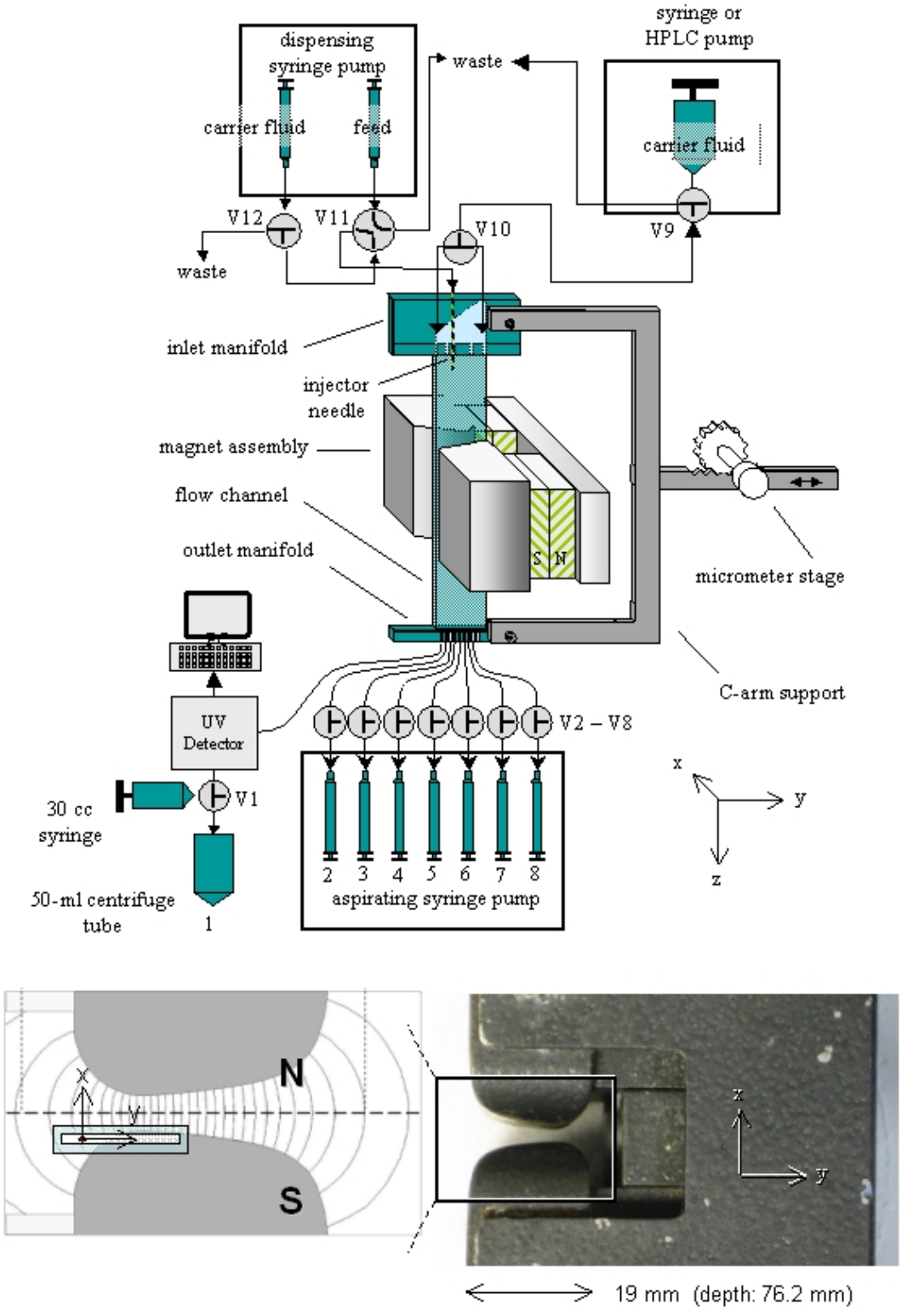

Figure S2. Top: schematic diagram of the of the dipole magnetic flow fractionator (DMF) system, where V stands for "valve" (three-way, as indicated). Bottom: photograph of the DMF interpolar gap showing Faraday pole pieces and a part of the associated permanent magnet. The diagram on the left shows relative position of the flow channel, with the coordinate axes fixed on the sample injector axis.

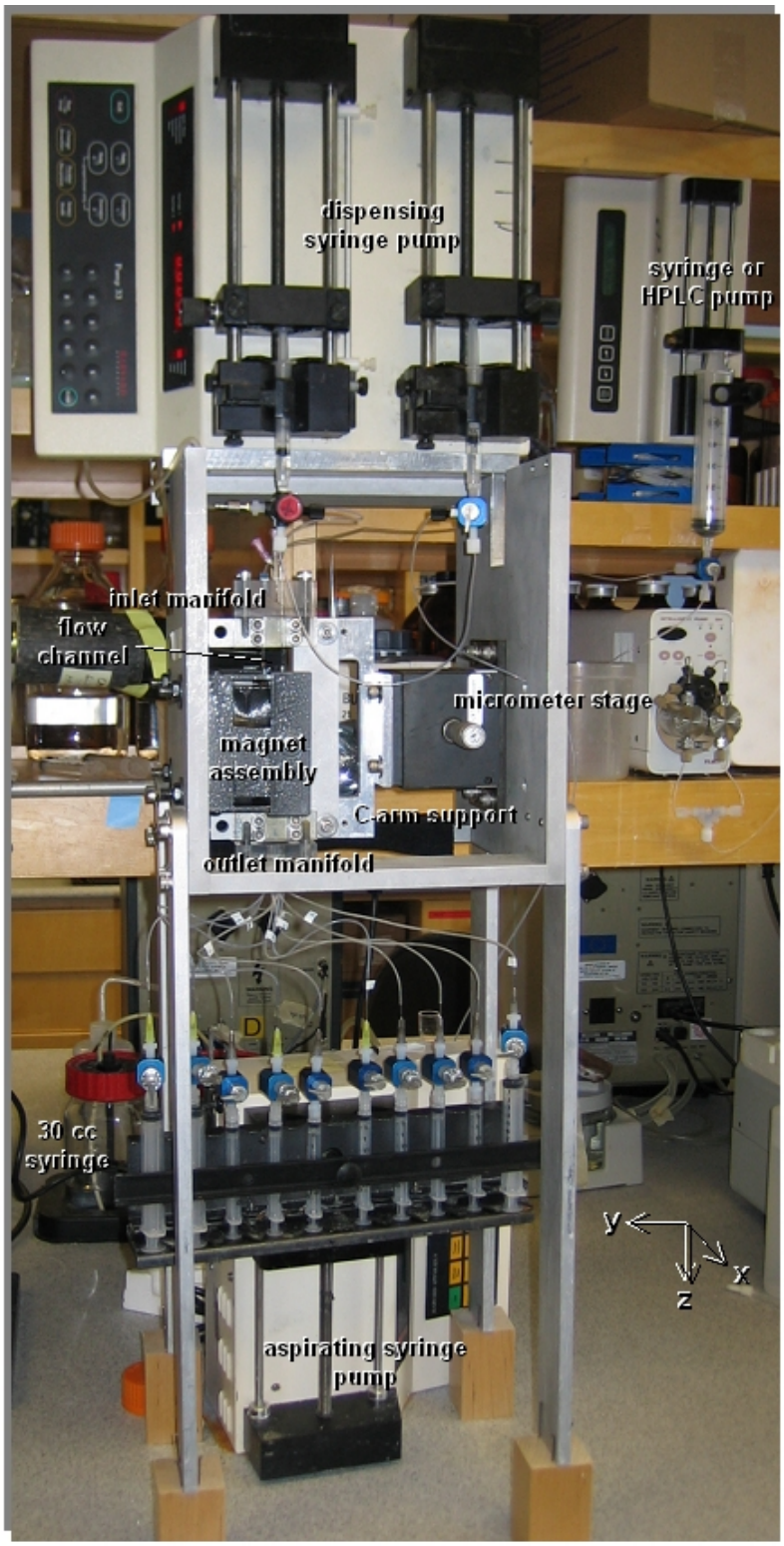

Figure S3. Photograph of one of the early versions of the DMF system (note ten rather than eight outlet tubings) showing essential components of the system.

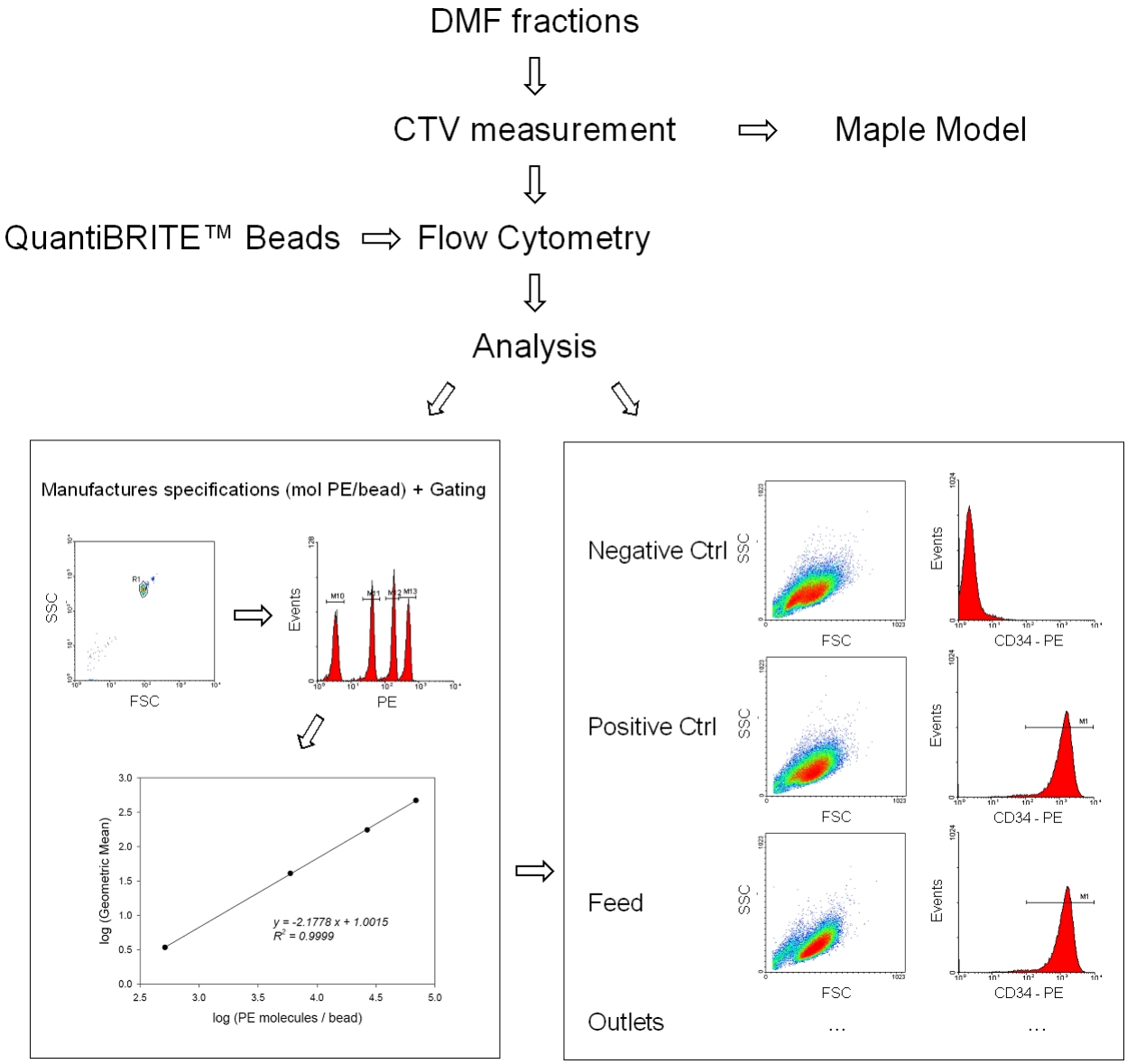

Figure S4. Flow chart of data acquisition.

Table S1. Increments to transport lamina thickness, Δb_t, in the system configurations tested.

Setup	A	B	C	D
Outlet		d_s [mm]		
1	1.917	1.917	1.918	1.918
2	0.398	0.354	0.300	0.246
3	0.399	0.354	0.300	0.246
4	0.399	0.354	0.300	0.246
5	0.399	0.354	0.300	0.246
6	0.399	0.354	0.300	0.246
7	2.505	1.986	1.465	2.406
8	2.435	3.177	3.986	3.295

Outlet syringe setup. Syringe size given for BD plastic – (outlet 1), (outlets 2-6), (outlet 7), (outlet 8): A= (17.88 mm), 5 × 3cc, 30cc , (2 × 10cc); B= (19.13 mm), 5 × 3cc, (2 × 10cc), (3 × 10cc); C= (20.62 mm), 5 × 3cc, 20cc, (2 x 30cc); D= (22.75 mm), 5 × 3cc, (2 × 20cc), (2 × 30cc).

Table S2. Resolution between outlets based on measured magnetophoretic mobility and fluorescent intensity.

Setup	A	B	C	D
Outlets	$R_{S,\,m}$, $R_{S,\,FI}$			
1 – 2	0.23 , 0.75	0.32 , 1.51	0.10 , 0.74	0.15 , 0.35
2 – 3	0.02 , 0.10	0.14 , 1.09	0.01 , 0.78	0.04 , 0.54
3 – 4	0.02 , 0.71	0.18 , 0.68	0.09 , 0.62	0.08 , 0.52
4 – 5	0.08 , 0.61	n/a , n/a	0.06 , 0.28	0.03 , 0.19
5 – 6	n/a , 1.16	n/a , n/a	n/a , 0.59	n/a , 0.43
5 – 7	0.08 , n/a	n/a , n/a	0.13 , n/a	0.17 , n/a
6 – 7	n/a , -0.43	n/a , n/a	n/a , 0.57	n/a , 0.06

n/a = not applicable.

Table S3. Resolution between outlets based on magnetophoretic mobilities from the Maple Model.

Setup	A	B	C	D
Outlets		$R_{S,\ m\ (Maple\ Model)}$		
1 – 2	0.228	0.184	0.208	0.190
2 – 3	0.148	0.146	0.108	0.105
3 – 4	0.189	0.193	0.153	0.100
4 – 5	0.179	0.172	0.149	0.110
5 – 6	0.137	0.132	0.144	0.127
6 – 7	0.207	0.177	0.218	0.235
7 – 8	0.615	0.376	0.329	0.528